THEORETICAL AND EXPERIMENTAL INVESTIGATIONS OF THE PHYSICS OF CRYSTALLINE SURFACES

Principal Investigator: E. Bauer

First Quarterly Report
For the Period February 1, 1966 to April 30, 1966

Prepared for the

National Aeronautics and Space Administration
Washington, D. C.

Fund Transfer R-05-030-001

U. S. Naval Ordnance Test Station
China Lake, California

First Quarterly Status Report
Fund Transfer No. R-05-030-001
For the Period 1 February-30 April 1966

I. The relation between structure of epitaxial films and surface and interfacial energies (A. K. Greer and E. Bauer).

Most of the effort was concentrated on evaluating the extensive experimental material collected during part of the last contract period and to prepare the material for publication. The publication will consist of two parts, one of which is finished (Encl. (1)). The second, theoretical, part is still in preparation and will be enclosed in the second quarterly progress report. Simultaneously with this work the experimental setup is being modified to allow the planned quantitative work under well defined experimental conditions.

II. Quantitative studies of the elastic and inelastic interactions of slow electrons with W single crystal surfaces (J. O. Porteus).

The principal effort in connection with the direct-scanning LEED instrument is now being directed toward preparation of clean, step-free tungsten (110) surfaces to be used for diffracted-beam intensity measurements. The work on identification and elimination of residual contaminants in the ultrahigh vacuum system is progressing satisfactorily. Better methods of orienting and cutting single crystals to minimize formation of surface steps are also being investigated.

A secondary effort involves development of an electronic programming and voltage control system to permit automatic tracking and intensity measurement of diffracted electron beams as the electron wavelength is varied. A system having sufficient flexibility to permit tracking at both normal and non-normal incidence has been designed and is now in the initial test stage.

III. Determination of nature and structure of surface layers with low energy electron diffraction (E. Bauer).

The important question of surface reconstruction has been reconsidered on the basis of a letter by L. H. Germer to Surface Science (see Encl. (2)).

IV. Relation between structure and electron emission properties of work function reducing layers on W{110} planes (G. Turner and E. Bauer).

Preliminary work has been done with SrO layers using the ultrahigh vacuum photoemission and mirror microscope, photocurrent, photoelectric work function, and contact potential measurements and low energy electron diffraction. The results are summarized in Encl. (3).

V. Momentum exchange of atoms on well defined single crystal surfaces (W. Faith and E. Bauer).

Most of the accessories needed to do the momentum exchange measurements in the low energy electron diffraction system have been designed and/or constructed.

PUBLICATIONS

1. "On the Formation of Single Crystal Films of f.c.c. Metals on Alkali Halide Cleavage Planes. I. Experimental Investigations in Ultra-high Vacuum," K. Kunz, A. K. Green, and E. Bauer, to be submitted to phys. stat. sol.

2. "The Uncertainty Regarding Reconstructed Surfaces," E. Bauer, to be published in Surface Science.

3. "An Ultrahigh Vacuum Electron Microscope and Its Application to Work Function Studies," G. Turner and E. Bauer, to be published in Proc. Sixth Internat. Congr. Electron Microscopy.

On the Formation of Single Crystal Films of f.c.c. Metals on Alkali Halide Cleavage Planes

I. Experimental Investigations in Ultrahigh Vacuum

K. M. Kunz, A. K. Green, and E. Bauer
Michelson Laboratory, China Lake, California 93555

ABSTRACT

Thin films of Au, Al, and Ag are evaporated in an ultrahigh vacuum reflection electron diffraction unit onto NaCl, KCl, and KI {100} surfaces cleaved in air and in situ. Their structure is studied by reflection diffraction during and after deposition, and by transmission electron diffraction microscopy. The results of simultaneous evaporation onto crystals with different surface condition (air versus vacuum cleaved) or composition show that the different stages of film growth (mainly nucleation and coalescence) depend in a complicated manner upon surface condition and composition. Electron irradiation prior and during deposition, preannealing of the air cleaved surface and annealing of the film after deposition strongly influence the film structure.

Dünne Au, Al, und Ag Schichten werden in einer Ultrahochvakuum-Elektronenbeugungsapparatur auf NaCl, KCl, und KI {100}-Flächen aufgedampft welche in Luft und in situ gespalten wurden. Die Schichtstruktur wird während und nach der Bedampfung mit Reflexionsbeugung untersucht, sowie mit Durchstrahlungsbeugungsmikroskopie. Die Ergebnisse von Simultanbedampfungen auf Kristalle mit unterschiedlichem Oberflächenzustand (in Luft bzw. in Vakuum gespalten) oder verschiedener Zusammensetzung zeigen dass die verschiedenen Wachstumsstadien (haupsächlich Keimbildung und Koaleszenz) in komplizierter Weise vom Oberflächenzustand und der Zusammensetzung abhängen. Elektronenbestrahlung vor und während der Bedampfung, Tempern der in Luft gespaltenen Oberflächen und der Schichten nach der Bedampfung haben starken Einfluss auf die Schichtstruktur.

1. INTRODUCTION

Since Lassen's discovery in 1934 [1] that single crystal Ag films could be grown by evaporating Ag onto a heated NaCl cleavage plane, numerous experimental and theoretical investigations have been made to obtain an understanding of the formation of single crystal films on single crystal substrates [2,3]. Nevertheless complete agreement between experiment and theory has not been achieved. The recent experimental observations of the influence of residual gases and surface layers on the film growth [4-16], suggest that the gap between theory and experiment is wider than had been assumed. This paper attempts (1) an experimental examination of some of the ideas put forward to explain the recent experiments just mentioned (Part I), and (2) a discussion of the theoretical implications of recent experimental results (Part II). In particular, the significance of nucleation and of coalescence for the film orientation will be critically analyzed. The reason for this is that in the most generally accepted theories of single crystal film formation, nucleation plays a central role and coalescence is neglected. Volmer and Weber suggested in 1926 [17] that the oriented growth of one crystal on another can be explained by differences in nucleation probability due to the variation of the interfacial energy between the two crystals with their relative orientation. Bauer [18] put this idea in a mathematical form and discussed critically the assumptions on which it is based. One of these assumptions is that the nucleus and the subnuclear clusters can be characterized by thermodynamic quantities such as specific free surface and interfacial energies. These quantities depend however, on cluster size and shape, in contrast to homogeneous nucleation

theory where they are constant. Bauer found that the relative number and shapes of differently oriented LiF crystals grown epitaxially on alkali halide cleavage planes could be explained in terms of nucleation theory only if the size and shape dependence of the interfacial energies σ_i was taken into account. Niedermayer [19] applied the theory to the epitaxy of Ag on NaCl and obtained rough agreement between observed and calculated epitaxial temperature. Pound and Hirth [20-22] later formulated the theory in terms of the liquid-like nucleus model, neglecting the size and shape dependence of σ_i, but including quantum statistical contributions important for absolute nucleation rates. They concluded that most of the qualitative aspects of epitaxy may be understood in terms of nucleation theory. Both approaches [18,20-22] are physically meaningful only if the clusters are so large that thermodynamic quantities can be ascribed to them. In general however, this is not true in the growth of single crystal films. The absolute numbers of nuclei are so large that according to the theory the nuclei consist of only a few atoms, if the macroscopic values for the specific free surface energies are used and the quantum statistical contributions are neglected. Walton [23] has therefore developed a statistical mechanical theory of epitaxy in which the nuclei consist of only a few atoms and in which the phenomenological quantities such as chemical potential or surface energy are replaced by atomistic quantities such as the binding energy between the atoms in the cluster and between cluster and substrate. Walton et al. [24] find that this theory explains quantitatively their observations of the absolute nucleation rates of epitaxial Ag deposited in ultrahigh vacuum onto NaCl cleavage planes. All of these nucleation theories agree in one basic assumption: the nuclei are assumed not to rotate but to

have a well defined orientation (or orientation distribution) which determines the orientation of the single crystal film. Recent experiments [4-16] which will be discussed in II indicate however that the orientation of the continuous film may be completely different from that of the nuclei. Also the absolute nucleation rates depend in a much more complicated manner upon experimental conditions than predicted by the nucleation theories.

2. Experimental Set-up and Procedures

All experiments were performed in an ultrahigh vacuum grazing incidence electron diffraction unit (Fig. 1), which allowed the examination of the substrate surface before film deposition and the observation of the film structure during and/or after deposition. As the design of the instrument differs somewhat from conventional electron diffraction units it will be described briefly. The electron gun was a television gun assembly with an oxide cathode mounted on an octal feedthrough ConFlat flange, which was at high voltage (generally 15 kV). Both electrostatic and magnetic focussed guns were used in the course of the experiments, the best giving spot diameters of .2 mm on the fluorescent screen, which was 46 cm from the cathode. The gun flange was insulated from ground by a pyrex tubing sealed to ConFlat flanges. The main body of the instrument with an I.D. of 6.3 cm had 12 ports around its periphery for mounting the specimen holder, cleaver anvil, evaporator, observation windows, shutter motion, quartz oscillator feedthrough, mass spectrometer, ionization gauge, pump connections, and gas inlet. An extension tube with the same I.D. provided a specimen-screen distance of 23.5 cm. The fluorescent screen was an aluminized ZnS screen on a thin glass plate and could be observed through a housekeeper sealed

window. The diffraction pattern was recorded with an oscilloscope camera using ASA 3000 Polaroid film. The all stainless steel system was sealed with copper gaskets.

The pumping system consisted of a mechanical and an oil diffusion pump for forepumping, a 40 ℓ/sec Vacion pump and a 50 ℓ/sec titanium getter pump for high vacuum pumping. Pumping system and diffraction chamber were connected with a low conductance line which reduced the pumping speed considerably but eliminated at the same time pressure differences between specimen and ion gauge location. The system was usually baked for five hours within which a maximum temperature of 250°C was reached. The lowest base pressure achieved was $3 \cdot 10^{-10}$ torr, with the electron gun operating the pressure rose typically to $5 \cdot 10^{-9}$ torr; the highest pressure during the experiments under the most unfavorable conditions (high evaporator power input, high specimen temperature) was $5 \cdot 10^{-7}$ torr. In general the pressure during evaporation did not rise above the middle 10^{-8} torr range. The residual gas composition, as measured with a CEC 21-612 residual gas analyser, varied with the operation mode of the system. The background gas, e.g. at a total pressure of $2 \cdot 10^{-9}$ torr consisted mainly of H_2, followed by CO, H_2O, CO_2, and CH_4. When the electron beam was on after thorough outgassing of the gun H_2 was dominating, followed by H_2O. With a hot NaCl specimen (e.g. 330°C, total pressure $2.5 \cdot 10^{-8}$ torr), H_2O was dominating (H_2 was not measured); hot KCl specimens outgassed less, but no gas analysis was made. The pressure increase during gold evaporation was mainly due to the strong CO evolution from gold.

The evaporators were W coils mounted on a four-lead press which allowed thorough outgassing of the leads. The evaporating material (> 99.5% Au,

99.999% Al, > 99.5% Ag) was melted down before the evaporation with the shutter closed and/or the specimen pointed away from the evaporator. Several evaporations were made with the deposition rate monitored by a Sloan quartz oscillator; it was found that the qualitative aspects of the film growth were not greatly influenced by deposition rate variations. Therefore most evaporations were made without rate monitoring. An approximately constant deposition rate was maintained by keeping the evaporator current constant and by varying it whenever redistribution of the evaporant made a power input change necessary. The average deposition rate as determined from deposition time and film thickness was varied from about 1 Å/min to about 1000 Å/min (except in wedge evaporations where in the thin end much lower rates were encountered). The evaporator-specimen distance was 5 cm. The specimens (Harshaw NaCl, KI, Leitz KCl) were held in a specimen holder which had bifilar heating coils and was made initially of OHFC copper, later of 304 stainless steel and finally of beryllium-copper. No influence of the specimen holder material on the results was noted, although stainless steel tended to outgas strongly above 350°C. The specimen temperature was measured with a fine (.003" diam. wire) iron-constantan thermocouple inserted into a fine hole drilled into the side of the crystal near its front face. The crystals could be cleaved in situ by pushing the specimen holder--which was mounted on bellows--including a stellite blade inserted into it, against an anvil opposite to the specimen holder. The specimen holder allowed lateral motion of the specimen, tilting, and to a limited degree a change in azimuth. All in situ electron diffraction investigations were made in or near the ⟨110⟩ azimuth. Electromagnetic deflection allowed the positioning of the beam conveniently anywhere on the

specimen making rapid examination of different specimen areas possible. The specimen surface was 0.3 x 1.2 cm^2 if only one crystal was used, 0.2 x 1.2 cm^2 when two crystals (e.g. NaCl and KCl) were used simultaneously.

Several deposition procedures were used: (1) deposition of wedge films on air cleaved or vacuum cleaved surfaces, (2) simultaneous deposition of a film with constant thickness onto (a) one or (b) two crystals, each of which consisted of an air cleaved and a vacuum cleaved half. The wedge films were made by evaporating from a line source perpendicular to the edge of a shutter properly placed between evaporator and specimen to obtain a sufficiently wide half shadow region. For the simultaneous depositions onto air and vacuum cleaved surfaces, the crystals were first sawed part way through, then placed into the specimen holder and one half was cleaved in air. The specimen was then turned around so that the uncleaved half faced the blade. This ensured that the thickness of the air cleaved half was the same as that of the half which was cleaved in vacuum shortly before evaporation. As a consequence both surfaces had the same temperature and could be scanned with the electron beam without readjusting the specimen holder. As difficulties were encountered sometimes in cleaving at the higher deposition temperatures (generally 260 - 360°C), the crystals were generally cleaved at 100°C - 200°C. Before cleaving the specimen holder was heated for several hours at the deposition temperature for outgassing and to establish the equilibrium impurity layer on the air cleaved side of the crystal. Deposition was started when the specimen had reached the desired temperature, 20 to 50 min after cleaving. Deposition times were between 10 sec and 30 min depending upon desired mean thickness (several Å

to about 1000 Å) and rate. Optical transmission was used as a rough criterion for the film thickness. This method gives only a very qualitative characterization because of the dependence of transmission upon the state of coagulation of the film. The procedures for electron diffraction examination of the film structure were varied in order to diminish and/or determine the influence of the electron beam on the film growth: sometimes the diffraction pattern was observed only after completion of the deposition, sometimes it was observed intermittently and sometimes it was monitored continuously. After deposition the specimen heater current was in general turned off immediately, allowing the specimens to cool to 200°C within 10 min and to 50°C within an hour. After removal from the system the evaporated films were stabilized with carbon and prepared for transmission electron diffraction microscopy in a JEM-5Y electron microscope.

In a number of experiments the experimental conditions deviated from those generally used as described above. This was done to obtain information on the possible influence of artefacts: (1) some crystals were heated at 360°C or higher for periods up to 48 hours before deposition to determine the influence of the preheating time on the film growth on air cleaved surfaces, (2) some crystals were held at the deposition temperature up to several hours after deposition to determine the influence of the annealing time on the film structure, (3) one very thin film was cooled to room temperature, exposed to air and examined again with reflection electron diffraction to determine the influence of exposure to atmosphere on the orientation in very thin films, (4) several evaporations were made at room temperature and above 400°C. A total of 72 evaporations were made (including the abnormal ones) of which 47 were of Au on NaCl, 7 of Au on KCl, 8 of Au on NaCl and KCl simultaneously, 6 of Al on NaCl, 3 of Ag on KCl and 1 of Au on KI.

3. Experimental Results

3.1. Nomenclature

The following nomenclature will be used to describe the various crystal orientations in the deposited films "D" on the various substrates "S".

(1). (100) stands for the parallel growth: $(100)_D \parallel (100)_S$, $[010]_D \parallel [010]_S$.

(2). (100)-45 stands for $(100)_D \parallel (100)_S$, $[010]_D \parallel [011]_S$.

(3). (111)[011] stands for $(111)_D \parallel (100)_S$, $[01\bar{1}]_D \parallel [01\bar{1}]_S$, $[0\bar{1}1]_S$, $[011]_S$ or $[0\bar{1}\bar{1}]_S$.

(4). (111)[001] stands for $(111)_D \parallel (100)_S$, $[0\bar{1}1]_D \parallel [001]_S$, $[00\bar{1}]_S$, $[010]_S$ or $[0\bar{1}0]_S$.

(5). (100)-T1 stands for the four primary twins along {111} of the parallel orientation (1), (100)-T2 for the secondary twins.

(6). (111)-T1 stands for the three primary twins along {111} of the eight (111) orientations (3), (4), (111)-T2 for the secondary twins.

(7). (211)[011] stands for $(211)_D \parallel (100)_S$, $[01\bar{1}]_D \parallel [011]_S$ or $[01\bar{1}]_S$.

(8). (211)[001] stands for $(211)_D \parallel (100)_S$, $[01\bar{1}]_D \parallel [001]_S$ or $[010]_S$.

(9). $(211)_{111}$ stands for $(211)_D \parallel (100)_S$ with the $[01\bar{1}]$ direction parallel to the $[01\bar{1}]$ directions of the (111)[011] orientations (3).

(10). (110) stands for $(110)_D \parallel (100)_S$ with the $[001]_D$ rotated $\pm$ 32.5° with respect to $[010]_S$ and $[001]_S$.

(11). (111)-I stands for the (111) one degree orientation with $(111)_D \parallel (100)_S$.

(12). (211)-I stands for the (211) one degree orientation with $(211)_D \parallel (211)_S$.

The environment of the crystal during cleavage is characterized by air, vac, UHV and (UHV). Air refers to cleavage in air of varying degrees of humidity (in our experiments 30 - 40%), vac refers to cleavage in ordinary unbaked

vacuum systems (10^{-4} - 10^{-7} torr total pressure), UHV refers to cleavage in baked ultrahigh vacuum systems ($p \lesssim 10^{-8}$ torr) and (UHV) refers to cleavage in unbaked UHV systems ($p \lesssim 10^{-7}$ torr). RED stands for reflection electron diffraction (for this work, in situ in UHV), TED for transmission electron diffraction, and TEM for transmission electron microscopy. No distinction will be made between twins, microtwins and stacking faults, all being called twins.

3.2. Wedge Evaporations

3.2.1. RED results

Wedge evaporations were made only for Au on air and UHV cleaved NaCl at 360°C and KCl at 270°C. In all four cases only a (100) orientation is observed in the thinnest parts of the wedges (Fig. 2a). The diffraction spots from the films on the UHV cleaved surface are however much sharper than those from films on the air cleaved surface, indicating a larger particle size. If the spot size on the air cleaved surface is attributed completely to particle size broadening, then the thinnest observable deposit consists of 10 Å diameter crystals. Similarly it can be concluded that the thinnest observable deposit on the UHV cleaved surface consists of particles at least 50 Å in diameter. The crystals on the UHV cleaved surface have a better azimuthal alignment than those on the air cleaved surface as determined from the intensity asymmetry when the electron beam is somewhat off the [011] direction. The alignment of the crystals increases with film thickness as indicated by the increase of the intensity asymmetry. With increasing thickness a weak (111) orientation develops of which only the (111) reflection is visible so that the azimuthal orientation

cannot be determined. Upon further increase in thickness the RED patterns become different for the various substrates. On air cleaved NaCl, air and UHV cleaved KCl the spots due to the (100) orientation develop streaks along the $\langle 111 \rangle$ directions and (100)-Tl spots appear (Fig. 2b). This is followed by the formation of streaks normal to the shadow edge (i.e. in the [100] direction) through the (100) orientation spots (Fig. 2c), a considerable increase in background, the complete disappearance of (111) orientation and the appearance of streaks between the Au diffraction spots normal to the shadow edge (in [100] direction) and with a distance of approximately $\frac{1}{5}\,[011]_{Au}$ (Fig. 2d). On a UHV cleaved NaCl surface the RED pattern observed with increasing film thickness is quite different. In addition to the (100) and (111) orientations strong approximate (211) orientations ((211)[011] or $(211)_{111}$) develop together with (100)-Tl and (111)-Tl (Fig. 2e). The spots of the approximately (211) oriented crystals which have their $[01\bar{1}]$ direction parallel to the electron beam are sharp while those from crystals with their $[01\bar{1}]$ directions perpendicular to the electron beam are split into spots which are streaked in $\langle 112 \rangle$ directions. With increasing film thickness the background increases strongly, the (100) orientation becomes weaker, the approximate (211) orientations disappear and strong (111)[011] orientations with spots strongly streaked normal to the shadow wedge ([111] direction) dominate the diffraction pattern. These qualitative variations in film structure across the wedge are not due to the variation in deposition rate across the wedge, but result from the thickness variation. This follows from the fact that on air cleaved NaCl, air and UHV cleaved KCl the RED pattern from a given specimen area when monitored carefully during deposition changes in the same manner with time

as it changes after deposition if scanned across the wedge. This is not true for the growth on UHV cleaved NaCl where the electron beam influences the film growth considerably even at the lowest useable currents (see 3.5.2.). In order to observe the film structure during deposition the irradiated area has to be changed frequently. This was done in some films of constant thickness (3.3), confirming the wedge results.

3.2.2. TED and TEM results

The TED results for the thin parts of the wedges, while qualitatively in agreement with the RED results, indicate that many details have been missed in the RED studies, mainly because they were done only in one azimuth ([011]) and its environment. The TED pattern from the thinnest part of the wedges studied in RED is obliterated by the diffuse pattern of the carbon film. The thinnest film which produces a TED pattern consists mainly of (100) oriented crystals with poor azimuthal alignment but contains also crystals with other poorly pronounced orientations. The contrast in the TEM pattern is too low to allow the determination of the crystal shape. With increasing film thickness--the crystals still being well separated--the azimuthal alignment of the orientations improves considerably, so that the orientations can be identified. The following weak orientations are found in addition to the strong (100) orientation: (111)[011], (110), (211)[011], (211)[001], (100)-Tl, (111)-I, (112)-I. The relative intensities of these orientations vary considerably from film to film, but on KCl the (211)[011], (211)[001] and (110) are the strongest; the (211)[011] orientation on UHV cleaved KCl is already visible in the thinnest part of the film. No major systematic orientation differences exist between films

on air cleaved and on UHV cleaved surfaces at this state, but the number of crystals is considerably smaller on the UHV cleaved surfaces than on the air cleaved surfaces. With increasing film thickness the number of crystals continues to increase, e.g. from $2.5 \cdot 10^{10}/cm^2$ to $15 \cdot 10^{10}/cm^2$ in the wedge shown in Fig. 3 a-e, the azimuthal alignment still improves somewhat, but no significant change in the relative intensity of the various orientations occurs until massive coalescence starts as indicated by a decrease of the number of crystals. From approximately this thickness until all crystals have some contact with each other the TED patterns differ considerably from the RED patterns, especially in the films deposited on UHV cleaved NaCl. The perfection of the orientation as indicated in the TED pattern is much poorer than suggested by the RED pattern. The (100)-Tl and (111)-Tl orientations are much stronger in TED than in RED. Although $(211)_{111}$ orientations are visible in the TED patterns of films on UHV cleaved NaCl, they are generally much weaker than expected on the basis of the RED patterns. Instead, the (111)[011] and (111)-Tl orientations appear strongly. When the films become partially continuous the discrepancies between TED and RED decrease and disappear nearly completely when the films become continuous. The films on air cleaved NaCl, air and UHV cleaved KCl assume pure (100) orientation with (100)-Tl orientations, the films on UHV cleaved NaCl exhibit (111)[011] and (111)-I orientations. A series of TED patterns of a wedge film on UHV cleaved KCl is shown in Fig. 3 f-j.

3.3. Simultaneous Evaporations on Air and UHV Cleaved Surfaces

3.3.1. Gold Films

The results for films deposited separately on NaCl and KCl agree substantially with those for films deposited simultaneously on NaCl and KCl. Therefore they are reported together.

Most of the very thin films, i.e. films with a mean thickness of less than 1 Å, were deposited at substrate temperatures below 300°C. In the thinnest deposits no condensation takes place on the UHV cleaved surface, while on the air cleaved surface many very small crystals grow. This difference in total condensation coefficient between air and UHV cleaved surfaces is still apparent after condensation has also taken place on the UHV cleaved surface. The number of crystals is much larger on the air cleaved surface than on the UHV cleaved surface while the average particle size is not very different. This is indicated in Fig. 4 a-d and in Table 1 which gives the particle numbers for two evaporations of Au onto NaCl and KCl and the average particle sizes and mean film thicknesses for one of these evaporations. The mean film thickness was determined from the particle size distribution and the assumption that all particles have (100) orientation and are four-sided pyramids bounded by {111} planes (see below).

The RED patterns show that the (100) orientation is dominant in very thin films and that its azimuthal perfection increases with film thickness. On the UHV cleaved surface the azimuthal alignment is better and the spots are sharper than on the air cleaved surface. This is confirmed by the TED study (see Fig. 4 e-h), which however reveals some weak subsidiary orientations which cannot be identified in the thinnest films because of the strong azimuthal misalignment. However in films of about 1 Å mean thickness the azimuthal alignment has improved sufficiently so that they can be identified. On UHV cleaved NaCl the (211)[011] orientations are strongest, followed by the (110) orientations and some (111)[011]. On air cleaved NaCl only (211)[011] orientations can be identified. On UHV cleaved KCl (211)[001], (211)[011], (110) and some (111)[011] are found, and on air cleaved KCl the

same orientations are noted but with the (111)[011] orientations stronger than the (110) orientations. The intensities of these subsidiary orientations vary somewhat from film to film.

The next important change in the film structure according to the wedge film studies occurs when major coalescence begins. The mean film thickness at which this happens varies with substrate temperature, deposition rate, and surface condition and lies between 10 Å and 100 Å for the temperature and deposition rate range studied. Major coalescence is indicated by a decrease in crystal number and an increase in crystal size and is accompanied by major changes in the crystal orientation as compared to that of the thinner films. The RED patterns of such films show that the intensity of the subsidiary orientations relative to the (100) orientation is lower than in the thinner films on air cleaved NaCl, air and UHV cleaved KCl and that the spots due to (100) orientation are streaked normal to the shadow edge. On UHV cleaved NaCl however the intensity of the (100) orientation is lower, the (111) orientations are stronger, but the dominant orientations are the approximate (211) orientations. The TED patterns of films on air cleaved NaCl, air and UHV cleaved KCl differ from the RED patterns in much stronger twinning and a much stronger intensity of the subsidiary orientations. The TED patterns of films on UHV cleaved NaCl differ considerably from the RED patterns in the relative intensity of the (111) and (211) orientations and by the appearance of strong (111)-T1 orientations which are sometimes not observed at all in RED. The TED patterns (Fig. 5 a-d) show that the (111) orientations are (111)[011] orientations with considerable azimuthal misalignment and some (111)-I orientation. The (211) orientations are $(211)_{111}$ orientations with similar azimuthal misalignment and some (211)-I orientation.

Typical electron micrographs of simultaneously deposited films in the coalescence stage are shown in Fig. 5 e-h. The island structure persists up to several hundred Å mean film thickness in the investigated parameter range, as does the discrepancy between RED and TED patterns of films on UHV cleaved NaCl. On the other surfaces the (100) orientation continues to become more and more important. At the same time the "1/5 streaks" normal to the shadow edge appear as mentioned above (3.2.1.).

The third significant stage in the film growth is reached when the islands have grown sidewards sufficiently to interconnect. In this state most of the subsidiary orientations have disappeared in the RED patterns. On air cleaved NaCl, air and UHV cleaved KCl only the (100) orientation with well pronounced "1/5 streaks" is visible. On UHV cleaved NaCl the (111) orientations are dominant. At large angles of incidence some approximate (211) orientation is observed in the thinner films but this orientation also disappears in continuous or nearly continuous films. In TED patterns some of the subsidiary orientations are visible even in the thickest films studied, especially in the films deposited below 300°C on UHV cleaved surfaces. An example is shown in Fig. 6. On both air cleaved surfaces the films are nearly continuous and have only (100) and (100)-Tl orientation. The films on the UHV cleaved KCl surfaces are more agglomerated and have some weak (111)[011] and (112) subsidiary orientations, while on UHV cleaved NaCl the film is still in the island stage and (100), (111)[011] and $(211)_{111}$ orientations are of comparable intensity together with strong (111)-I and (211)-I orientation. When the films become continuous the subsidiary orientations in films on UHV cleaved KCl disappear too and a (100) oriented single crystal film is formed with fewer imperfections than

in the films on the air cleaved surface. In films on UHV cleaved NaCl the $(211)_{111}$ orientation disappears and at 360°C only the (111)[011] orientations with poor azimuthal alignment and the (111)-I orientation remain (see Figs. 11k, 12h in ref. 12).

A number of films were deposited at room temperature. The RED pattern showed random orientation from the thinnest ($\lesssim$ 1 Å) to the thickest ($\sim$ 100 Å) films both on air cleaved and UHV cleaved surfaces. However the state of agglomeration differed considerably. At 190°C substrate temperature Au formed continuous films with (100) orientation on air cleaved KCl, however the films contain a much larger number of twins than those deposited at 270°C or 360°C. No depositions were made at substrate temperatures between 25°C and 190°C. One thick film was deposited onto KI at 260°C in order to obtain information on the origin of the "1/5 streaks". The films on both the air cleaved and UHV cleaved surface had (100) orientation in RED together with strong "1/5 streaks"; TED reveals only the (100) and the (100)-T1 orientations. The relative streak intensities indicate that the "1/5 streaks" are not due to a layer with the lateral spacing of approximately 5 $[011]_{Au}$ but result from double scattering between Au and a layer with a periodicity of about 5/3 $[011]_{Au}$ in the [011] direction of the Au crystals. Before the "1/5 streaks" were formed the diffraction spots were strongly streaked normal to the surface and in $\langle 311 \rangle$ directions.

3.3.2. Silver films

Only a few evaporations were made, the goal of which was to check the generality of the observations made with Au films. Only KCl was used as substrate. RED reveals the following sequence in film growth on the air

cleaved surface at 340°C. Initially (100), (111)[011], random and a number of subsidiary orientations are formed. With increasing film thickness the random and subsidiary orientations disappear and the (100), (100)-45 and (111)[011] orientations become dominant. Then the background increases suddenly, random orientation appears again and strong approximate (211) orientations form. Finally, (at several 100 Å thickness) only reflections due to the (111) orientations, streaked normal to the surface, are clearly visible on the strong background, with some weak indication of (100) and random orientation. On the UHV cleaved side the approximate (211) orientations are clearly visible above the strong background in the intermediate stage of film growth, as is the (111)[011] orientation with strongly streaked reflections at the end of the film growth. In no case are streaked spots due to the (100) orientation or "1/5 streaks" observed. TED and TEM showed that both films are very poorly oriented and consist of large isolated crystals. Ag films (approximately 100 Å thick) deposited at 200°C gave RED patterns with some preferred orientations which are superimposed on such strong rings that they could not be identified. The TED patterns show on the UHV cleaved surface some (111)[011], $(211)_{111}$, (111)-T1 in addition to the strong random orientation, on the air cleaved surface the (100) orientation is as strong as the random orientation. The crystal size and film thickness is much larger on the air cleaved surface than on the UHV cleaved surface. Ag films deposited at room temperature give RED patterns consisting of very broad rings and weak spots due to (111)[011] orientations.

3.3.3. Aluminum films

One Al film was deposited onto NaCl at 360°C, all others were deposited onto NaCl at 270°C. In all cases the first noticeable deposit in RED

consists of crystals with good (100) and (111)[011] orientations. The relative intensity of (100) to (111) orientations is much larger on the air cleaved than on the UHV cleaved surface; the first spots are much sharper and appear later on the UHV cleaved surface. In the very thin film deposited at 360°C no condensation takes place on the UHV cleaved surface. Fig. 7 shows the difference between very thin films deposited at 270°C on an air cleaved and a UHV cleaved surface. In the thinnest films (211)[011] orientations are observed in TED (especially on the UHV cleaved surface) in addition to the stronger (100) and (111)[011] orientations; all orientations have a misalignment of several degrees. The (211)[011] orientations are no longer observed in films which have coalesced, however some very weak $(211)_{111}$ orientations are present, especially on the UHV cleaved surfaces. With increasing coalescence the (111)[011] orientation becomes stronger, a (111)-I orientation develops and the (100) orientation becomes weaker. RED shows that when the (100) orientation is much stronger than the (111)[011] orientation (air cleaved surface) the reflections of the (100) orientation have strong streaks in the [100] and weak streaks in the ⟨111⟩ directions (Fig. 8a), while the reverse is true if the (111)[011] orientations are comparable in intensity to the (100) orientation (Fig. 8b). The rings and arcs due to (111) orientations in the TED patterns of Al consist always of sharp spots in contrast to those of Ag and Au which are always streaked in ⟨111⟩ directions. However the spots and arcs due to the (100) orientations have weak streaks in ⟨011⟩ directions.

3.4. Artefacts

3.4.1. Pretreatment and preheating

The treatment of the surface previous to deposition has considerable influence on the film growth. In the present experiments the exposure to air of the air cleaved surfaces before insertion of the specimen into the deposition system was in general less than 2 min, but the in situ treatment of the crystals (bakeout time, crystal preheating temperature and time, etc.) was varied. Some crystals were also vacuum annealed at 600°C for several hours before cleaving in air but no difference between films grown on such crystals and films grown on unannealed crystals was noticed. Also the bakeout time did not seem to influence the film growth. However the preheating of the crystal (for outgassing purposes) which was normally done at the deposition temperature, affected the film structure considerably. A thick gold film on air cleaved NaCl surface which had been kept at 360°C for 48 hours before deposition has the same structure as the film simultaneously deposited onto a UHV cleaved surface. Shorter annealing times at 360°C have correspondingly less influence, but even preheating for 5 hours is noticeable. Most experiments at 360°C were therefore performed with preheating times less than 3 hours. At 270°C no influence of the preheating time is noticed. Before the shutter was installed in the system condensation of Au was occasionally observed on the air cleaved surface resulting from the outgassing of the Au evaporator. This occurred although the surface was turned away from the evaporator, so that it could not see the Au source. These evaporations were excluded from the comparison.

3.4.2. Influence of the electron beam

The electron beam had in many cases a profound influence on the film growth when the surface was irradiated before or during deposition. The following effects are noted: (1) Roughening of the alkali halide surface either by locally varying decomposition or by recondensation of decomposed NaCl or KCl on the alkali halide surface or on the Au crystals. This gives rise to double scattering between the alkali halides and the Au crystals. (2). Increase in particle density in thin films and of the coverage in thick films. This is quite obvious from the optical transmission and from TEM pictures and is much more pronounced on UHV cleaved surfaces than on air cleaved surfaces as illustrated by the following examples: during slow deposition (20 min) of a thick Au film at 360°C onto NaCl the electron beam was intermittently aimed at the same specimen area. In one case this area was on the air cleaved surface and its transmission was only 3% as compared to 9% on the unirradiated part of the air cleaved surface and to 20% on the UHV cleaved surface. In another case this area was on the UHV cleaved surface and its transmission was only 2% as compared to 12% on the unirradiated part of the UHV cleaved surface and to 2% on the air cleaved surface. The optical transmission and TEM results indicate that the total condensation coefficient is larger in the irradiated area than on the unirradiated areas. (3). Change in crystal orientation, especially in Au films on UHV cleaved NaCl and in Al and Ag films. In all cases electron irradiation prior or during the initial stages of deposition favored the formation of (100) orientation. Therefore the effect is not so obvious in films which developed a (100) orientation also without irradiation (Au on air cleaved NaCl, air and UHV cleaved KCl), but is still noticeable in

an improvement of the orientation. On UHV cleaved NaCl the beam area in a thick film is found to have perfect (100) orientation with "1/5 streaks", while the unirradiated area has strong (111) orientations. In a thin Au film deposited at room temperature onto NaCl the beam area has a (100) orientation with somewhat arced spots while the rest of the film is randomly oriented. The beam area in the Ag film deposited at 270°C onto KCl shows a very good (100) orientation while the rest of the film is very poorly oriented (see 3.3.2). In the beam area of an Al film deposited onto NaCl at 270°C the orientation is nearly exclusively (100) with hardly any (111) orientations. All these orientation changes are observed under such weak irradiation that no roughening of the surface can be detected in the early stages of condensation. (4). The intensity of the (100)-Tl orientation in the early stages of the growth of Au films on NaCl and KCl seems to be somewhat higher in the irradiated area than in the unirradiated area. In the results reported in 3.2 and 3.3 we believe that the influence of the electron beam is eliminated by varying the irradiation conditions and/or by avoiding irradiation until after the deposition.

3.4.3. Annealing

If a thin film is not quenched to sufficiently low temperatures immediately after completion of the deposition, its structure may change considerably, as illustrated in the following examples. (1). A very thin Au film deposited on UHV cleaved NaCl at 450°C which showed a clear RED pattern with (100) orientation at the end of the deposition was left at 450°C for 30 min. Within this time the RED pattern becomes gradually weaker and disappears completely. Inspection of the crystal surface in

the light microscope shows that a few agglomerates too large to produce a RED pattern have been formed. (2). Au films in the coalescence stage consist of much larger particles if kept at the deposition temperature (360°C) for 30 min or longer than if cooled off immediately. (3). Continuous Au films deposited on UHV cleaved NaCl at 360°C exhibit considerable grain growth if kept at 360°C for several hours. The results reported in 3.2 and 3.3 refer to films which cooled off immediately after deposition (see 2). Because of the slow cooling rate (from 360° to 200°C in 10 min) slight annealing effects after deposition cannot be excluded.

3.4.4. Influence of atmosphere

Films deposited at elevated temperature were little influenced by exposure to atmosphere as judged by their RED pattern. A very thin Au film on NaCl which had poor azimuthal alignment was cooled to room temperature, exposed to air with 35% humidity for an hour and then reexamined by RED. No difference in the crystal orientation and its azimuthal perfection is observed. However thin Au and Ag films deposited onto NaCl and/or KCl at room temperature change drastically upon exposure to air. The TED and TEM results for these films were therefore discarded. The TED and TEM results for the films deposited at elevated temperatures are considered to be uninfluenced by exposure to atmosphere between deposition and TEM and TED sample preparation.

3.4.5. Preparation artefacts

In 3.2 and 3.3 it was pointed out that considerable discrepancies existed between the RED and TED patterns of films consisting of large isolated crystals and nearly continuous films up to several hundred Å

mean film thickness in the investigated parameter range. It seems reasonable to explain these discrepancies by the difference between the sensitivity of RED and that of TED. In a film with varying thickness RED detects preferentially the crystals sticking out of the surface while TED detects preferentially the thinner parts of the film if the thicker parts of the film absorb the beam sufficiently. We believe this explanation to be true for nearly continuous films but not for films consisting of large isolated islands for the following reasons: (1) in films with strong approximate (211) and weak (111) orientations according to the RED patterns, but weak (211) and strong (111) orientations according to the TED patterns, the approximate (211) orientations are dominant in the RED patterns even at the largest angles of incidence at which a RED pattern can be obtained. (2) Films consisting of large islands when stabilized with collodion have less $(211)_{111}$ orientation, more (111)[011], (111)-Tl, and random orientation than films stabilized with carbon. This suggests that carbon stabilization--although better than collodion stabilization--is not sufficient to keep the film from changing its structure upon removal from the substrate, a phenomenon well known from other work. That this phenomenon occurs only to a small extent or not at all in films consisting of very small crystals can be explained by the larger contact area and smaller lateral extension of the crystals. In nearly continuous films new surface area would have to be produced in order to obtain any major changes in film structure. However minor changes may still occur such as an increase in the number of twins.

3.5. Comparison and Summary of Experimental Results

A comparison of all experimental results (3.2–3.4) for the materials investigated gives the following picture of the film growth under our

experimental conditions. In the thinnest Au films the (100) orientation is always prominent, however has poor azimuthal alignment and is accompanied by a number of subsidiary orientations which are too weak to be detected in RED above the background due to the substrate. All crystals are well aligned with respect to the substrate normal. In TED the subsidiary orientations are noticeable even in the thinnest films. No (111) orientations are detected in the thinnest Au films. They are however quite apparent in the thinnest Al and Ag films, together with several subsidiary orientations which in the case of Ag films included random orientation. Condensation on the UHV cleaved surface is always delayed with respect to the air cleaved surface in the cases investigated (Au, Al). The crystals formed initially are considerably larger and better aligned azimuthally on the UHV cleaved surface than on the air cleaved surface and their number is much smaller. The difference in crystal size decreases with increasing film thickness so that the average size on the UHV cleaved surface is only slightly larger than on the air cleaved surface in Au films of about 1 Å mean thickness deposited at 270°C (90 Å versus 70 Å). On crystals of this size the shape can be clearly recognized: the (100) oriented Au crystals are four-sided pyramids formed by {111} planes, the (211) oriented crystals are rod-shaped, the few observed (111) oriented crystals are triangles or hexagons bounded by {111} planes and the (small) number of diamond-shaped crystals seems to be related to the intensity of the (110) orientations, which would indicate a {111} habit of these crystals. The mean thickness of thin films and the number of crystals on a UHV cleaved surface are considerably smaller than on the air cleaved surface in the cases studied (Au, Al), indicating a correspondingly lower total condensation

coefficient and nucleation rate on the UHV cleaved surface. However mean film thickness and number of crystals are nearly equal on UHV cleaved NaCl and UHV cleaved KCl surfaces. The film thickness can be considerably increased and the crystal orientation changed by electron bombardment.

With increasing film thickness the number of crystals and their average size increases without much change in the relative intensity of the various orientations but with an improvement in azimuthal alignment. In this stage the (100) oriented Au crystals develop in addition to the {111} faces (100) facets. On KI {311} facets instead of {111} facets are observed. In Al films the (100) oriented crystals on the air cleaved surface develop large (100) faces and small {111} faces. On the UHV cleaved surfaces the {111} faces are more pronounced than the (100) faces.

When the particle density becomes so high that many particles come into contact, massive coalescence occurs and the number of crystals decreases as their average size increases. At the same time major changes in the orientation film occur. In the RED pattern coalescence is accompanied by a strong increase in background irrespective of the surface condition. This is probably due to the increase in particle size but may also be caused by a large number of point imperfections which may be formed upon coalescence. Superimposed on the background of the Au films on air cleaved NaCl, air and UHV cleaved KCl and KI are the streaks of the (100) orientation and the "1/5 streaks" which increase in intensity from NaCl to KCl to KI. From the RED pattern of the film on KI it can be deduced that the 1/5 streaks are formed by multiple scattering between a thin single crystal surface layer with a periodicity of about $\frac{5}{3}\, d^{Au}_{011}$ in the [011] direction of Au and the Au crystals with (100) orientation. The directions of the streaks

indicate that on NaCl the crystals are bounded by (100) faces parallel to the substrate, while on KCl and especially on KI other faces are present on the surface of the film. No 1/5 streaks are formed in Ag films on KCl or Al films on NaCl. This suggests that the surface layer responsible for the "1/5 streaks" is a gold-alkali reaction product formed by reaction with the substrate, because Au is the only one of the three metals forming reaction products with the alkali metals, especially with K. The "1/5 streaks" are also not observed in Au films deposited on UHV cleaved NaCl, except in the irradiated area. Instead, strong approximate $(211)_{111}$ and (211)-I orientations form, just as in the unirradiated areas of Ag films on KCl. The spots in the RED pattern due to the approximately $(211)_{111}$ oriented crystals with their $[01\bar{1}]$ directions parallel to the electron beam are sharp while those with their $[01\bar{1}]$ directions normal to the beam are split into spots which are streaked approximately in $[2\bar{1}\bar{1}]$ and $[12\bar{1}]$ directions respectively. As the {211} planes are not equilibrium planes of the f.c.c. structure and not stacking fault planes the streaks are attributed to a small extension of the approximately $(211)_{111}$ oriented crystals in the approximate $[2\bar{1}\bar{1}]$ and $[12\bar{1}]$ directions, with the $(211)_{111}$ oriented crystal sandwiched between two differently oriented crystals. The differences between RED and TED patterns in this stage of the film growth are attributed to preparation artefacts. When the large crystals observed in this stage begin to contact each other the (111)[011] and (111)-I orientations become stronger at the expense of the approximate $(211)_{111}$ and (211)-I orientations. In continuous Au films deposited at 360°C only the (111)[011] and (111)-I orientations remain, at 270°C some of the other orientations also remain.

No continuous films were prepared of Ag and Al. Al films differ from Ag and Au films in that they form very little approximate (211) orientation upon coalescence. Annealing of continuous films at the deposition temperature leads to a considerable grain growth in the (111) oriented films and to a reduction in twin (or stacking fault) density in (100) oriented films.

This work was supported in part by the National Aeronautics and Space Administration under Contract No. R-05-030-001.

REFERENCES

[1] H. Lassen, Phys. Z. 35, 172 (1934).

[2] H. Mayer, Physik dünner Schichten, Vol. II, Wissenschaftliche Verlagsgesllschaft, Stuttgart, 1955.

[3] D. W. Pashley, Adv. Phys. 5, 173 (1956); 14, 327 (1965).

[4] S. Ino, D. Watanabe, and S. Ogawa, J. Phys. Soc. Japan 17, 1074 (1962); 19, 881 (1964); Acta Cryst. 16, A133 (1963).

[5] M. Harsdorff, Solid State Commun. 1, 218 (1963); 2, 133 (1964); Fortschr. Miner. 42, 250 (1966).

[6] C. Sella and J. J. Trillat, in Single Crystal Films, ed. by M. H. Francombe and H. Sato, Pergamon Press, Oxford, 1964 (p. 201).

[7] J. Jannet and C. Sella, Bull. Soc. franc. Minér. Crist. 87, 393 (1964).

[8] M. Harsdorff and H. Raether, Z. Naturforsch. 19a, 1497 (1964).

[9] J. W. Matthews and E. Grünbaum, Appl. Phys. Letters 5, 106 (1964); Phil. Mag. 11, 1233 (1965).

[10] J. W. Matthews, Appl. Phys. Letters 7, 31 (1965).

[11] S. Shinozaki and H. Sato, J. Appl. Phys. 36, 2320 (1965).

[12] E. Bauer, A. K. Green, K. M. Kunz, and H. Poppa, International Symp. Basic Problems in Thin Film Physics, Clausthal-Göttingen, Sept. 1965.

[13] H. Bethge and M. Krohn, International Symp. Basic Problems in Thin Film Physics, Clausthal-Göttingen, Sept. 1965.

[14] J. W. Matthews, Am. Vacuum Soc. Conf., New York, Oct. 1965; Phil. Mag. 12, 1143 (1965).

[15] A. K. Green and E. Bauer, J. Appl. Phys. 37, 917 (1966).

[16] E. Bauer, A. K. Green, and K. M. Kunz, Appl. Phys. Letters, to be published.

REFERENCES (Cont'd)

[17] M. Volmer and A. Weber, Z. Phys. Chem. 119, 295 (1926).

[18] E. Bauer, Z. Kristallogr. 110, 395 (1958).

[19] R. Niedermayer, Dissert. Clausthal 1963.

[20] G. M. Pound and J. P. Hirth, in Condensation and Evaporation of Solids, ed. by E. Rutner, P. Goldfinger, and J. P. Hirth, Gordon and Breach, New York, 1964 (p. 475).

[21] J. P. Hirth and G. M. Pound, Condensation and Evaporation, Macmillan, New York, 1963 (p. 41).

[22] J. P. Hirth, S. J. Hruska, and G. M. Pound, in Single Crystal Films, ed. by M. H. Francombe and H. Sato, Pergamon, Oxford, 1964 (p. 9).

[23] D. Walton, J. Chem. Phys. 37, 2182 (1962); Phil. Mag. 7, 1671 (1962).

[24] D. Walton, T. N. Rhodin, and R. Rollins, J. Chem. Phys. 38, 2695 (1963).

FIGURE CAPTIONS

Fig. 1. Ultrahigh vacuum electron diffraction apparatus, (for in situ RED observation of crystal growth).

Fig. 2. In situ RED patterns of wedge evaporation, see text.

Fig. 3 a - e. Wedge deposit of Au on UHV cleaved KCl at 280°C. Electron micrographs of increasing thickness along the wedge, X30,000.

Fig. 3 f - j. Wedge deposit of Au on UHV cleaved KCl at 280°C. TED patterns corresponding to Fig. 3 a - e.

Fig. 4 a - d. Simultaneous deposition of Au onto NaCl and KCl at 270°C, thin film. Electron micrographs of air NaCl, UHV cleaved NaCl, air KCl, and UHV cleaved KCl respectively, X30,000.

Fig. 4 e - h. Simultaneous deposition of Au onto NaCl and KCl at 270°C, thin film. TED patterns corresponding to Fig. 4 a - d.

Fig. 5 a - d. Simultaneous deposition of Au onto NaCl and KCl at 270°C, coalescence stage. TED patterns of air NaCl, UHV cleaved NaCl, air KCl, and UHV cleaved KCl respectively.

Fig. 5 e - h. Simultaneous deposition of Au onto NaCl and KCl at 270°C, coalescence stage. Electron micrographs corresponding to Fig. 5 a - d, X30,000.

Fig. 6 a - d. Simultaneous deposition of Au onto NaCl and KCl at 270°C, thick film. TED patterns of air NaCl, UHV cleaved NaCl, air KCl, and UHV cleaved KCl respectively.

Fig. 6 e - h. Simultaneous deposition of Au onto NaCl and KCl at 270°C, thick film. Electron micrographs corresponding to Fig. 6 a - d, X30,000.

FIGURE CAPTIONS (Cont'd)

Fig. 7. Electron micrographs of aluminum deposited onto NaCl at 360°C, X30,000. a, air and b, UHV cleaved.

Fig. 8. In situ RED patterns of aluminum deposited onto NaCl at 360°C. See text.

TABLE 1

Comparison of the crystallite number and size on air and UHV cleaved alkali halide surfaces

Film	Substrate	Temperature (°C)	Deposition Rate (Å/min)	Cleaving Environment	Number N of particles (in 10^{10}/cm^2)	Average particle diam. $\overline{D}$ (Å)	Mean film thickness $\overline{t}$ (Å)
Au	NaCl	270	~ .5	Air	25	70	2.2
				UHV	5	90	.8
	KCl			Air	20	70	2.0
				UHV	3.5	90	.5
Au	NaCl	270	~ 5	Air	100		
				UHV	4		
	KCl			Air	80		
				UHV	4		
Al	NaCl	270	~ 5	Air	13	180	
				UHV	3	180	

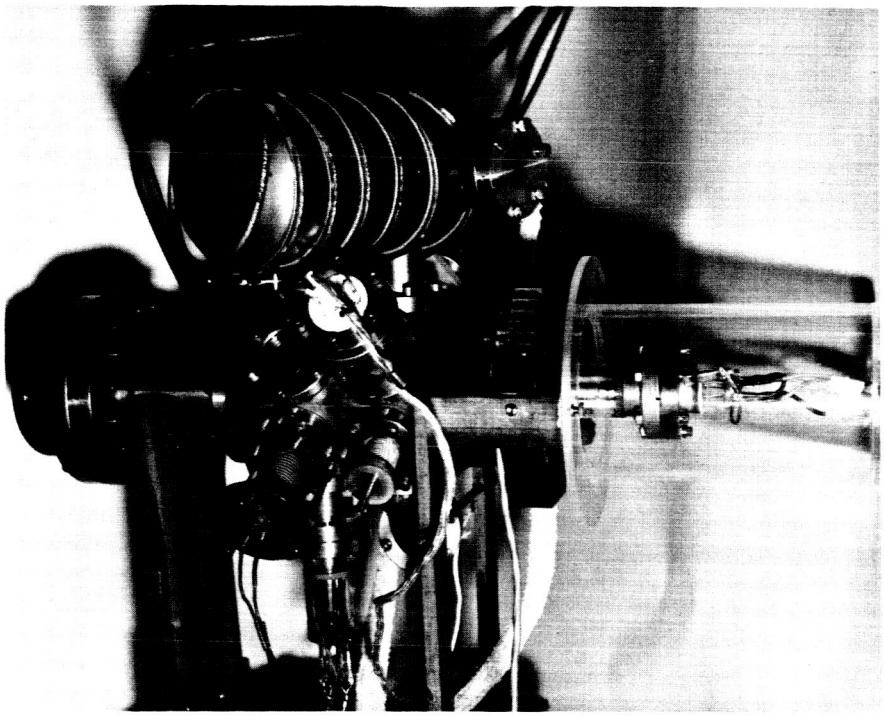

Fig. 1

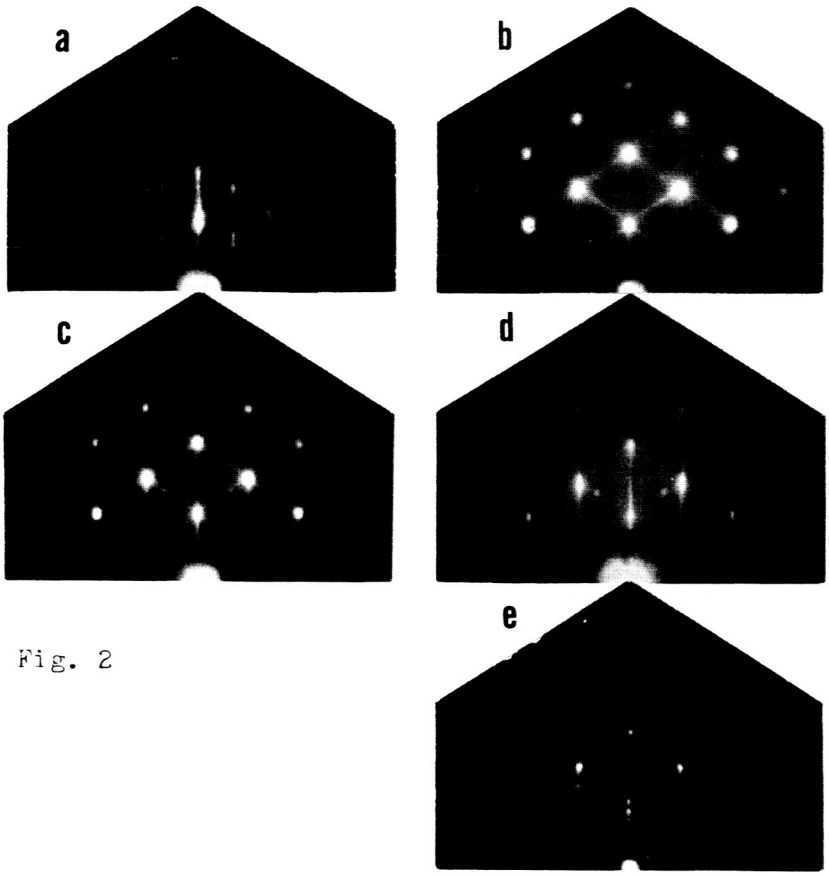

Fig. 2

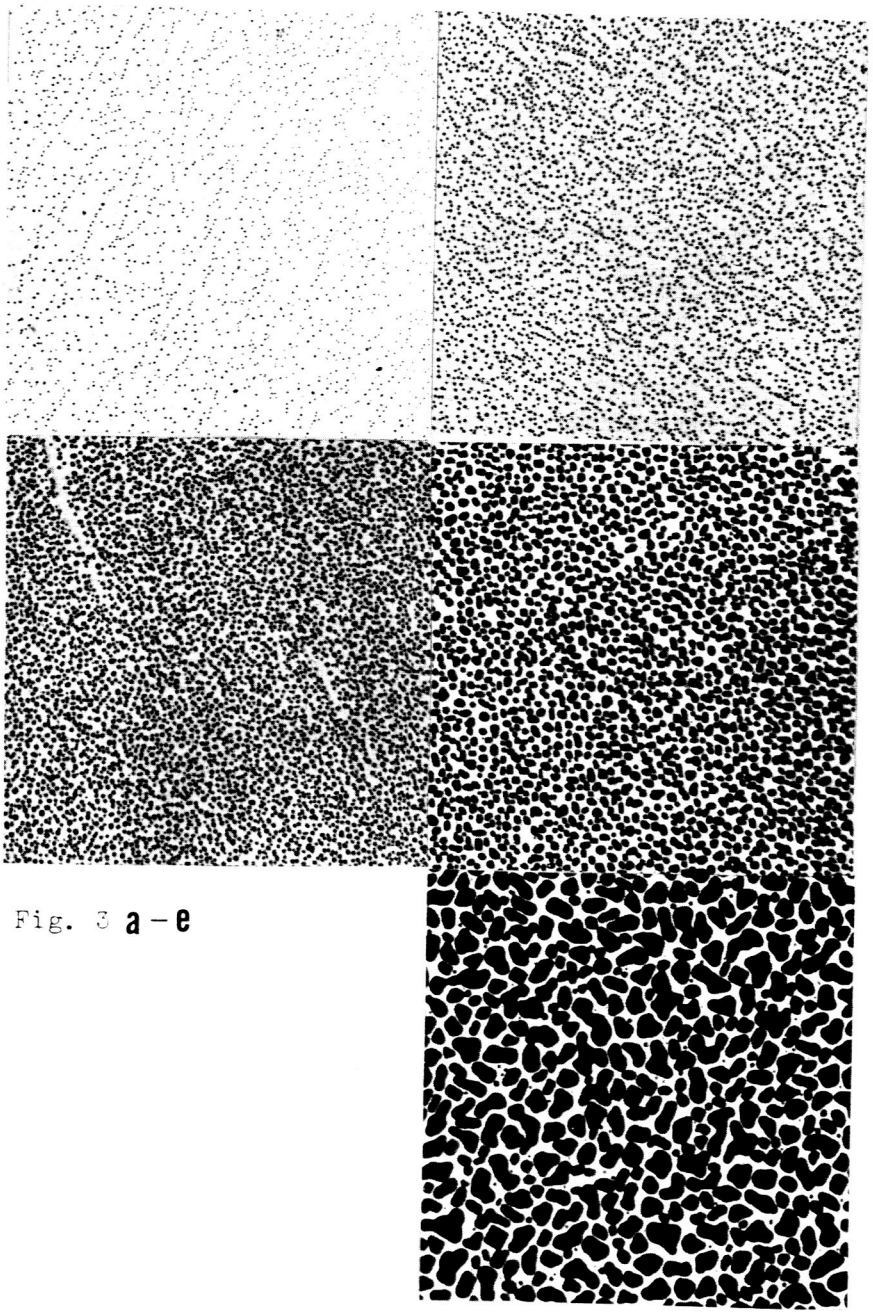

Fig. 3 a – e

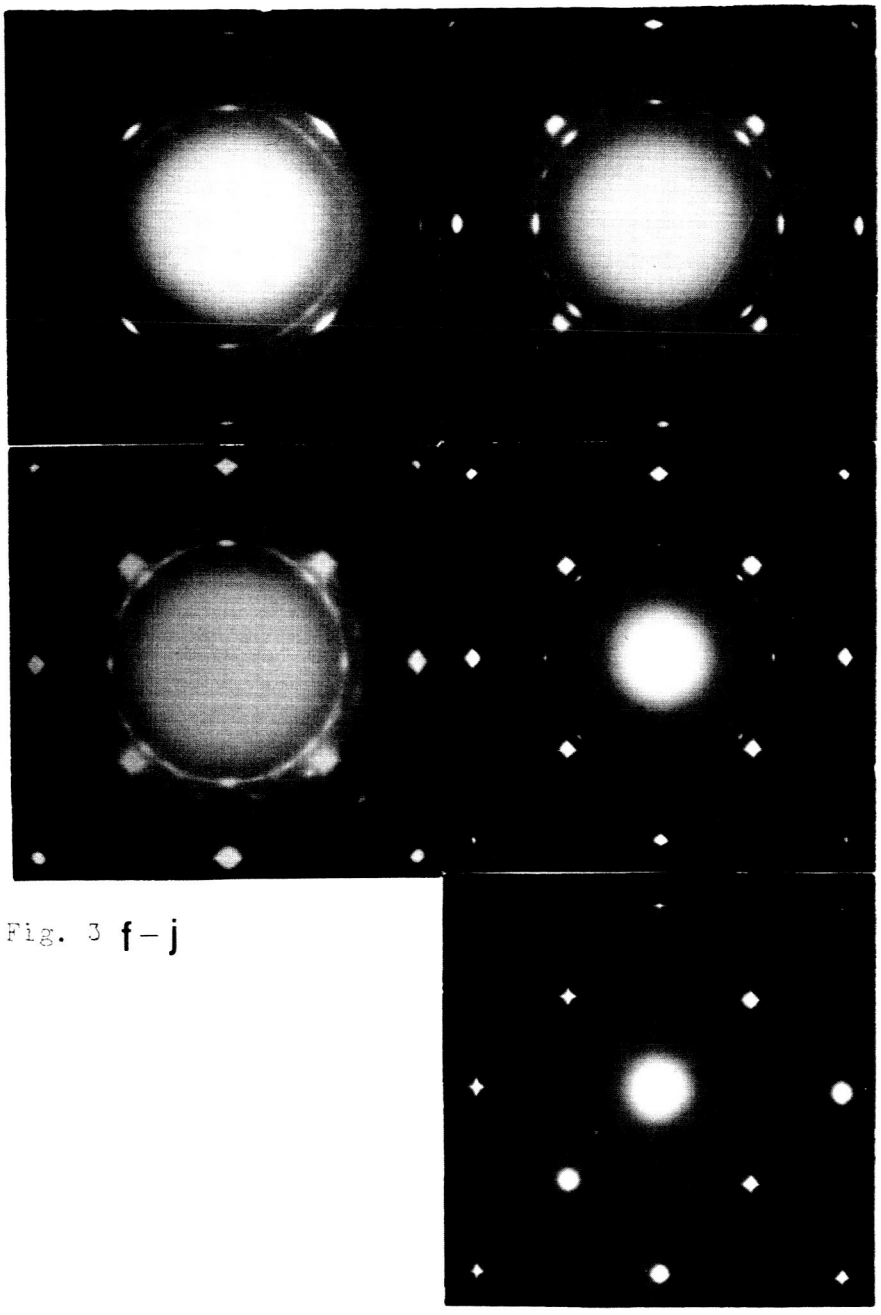

Fig. 3 f – j

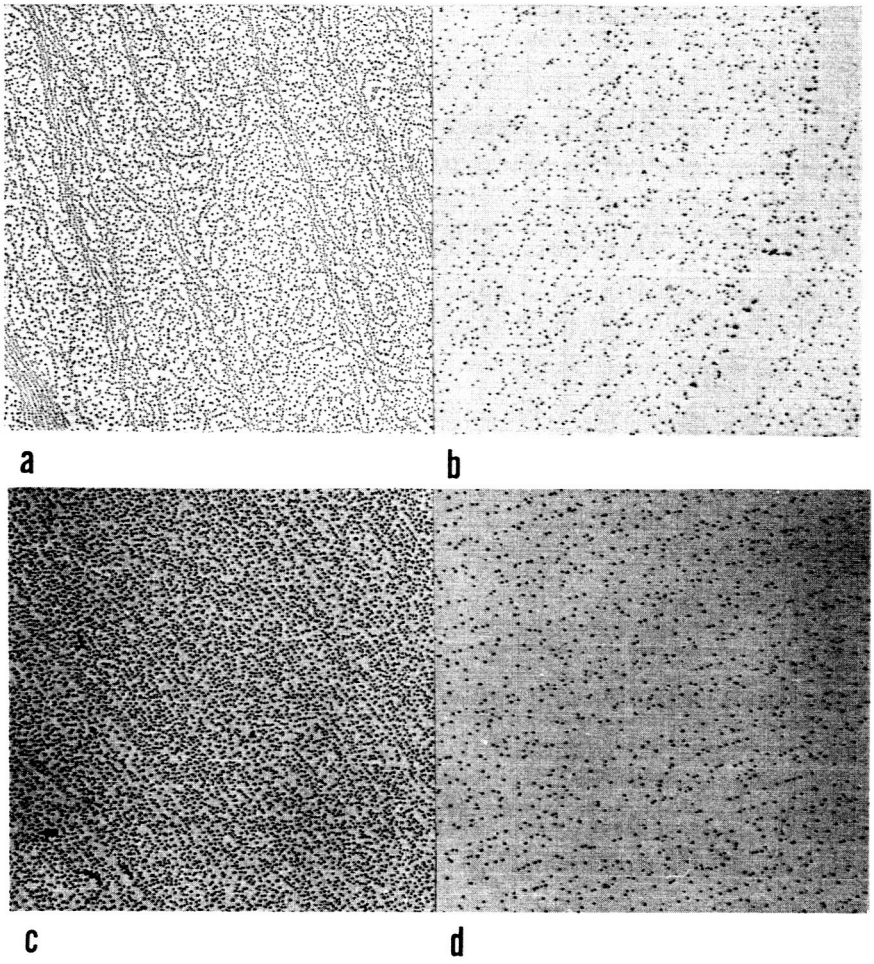

Fig. 4

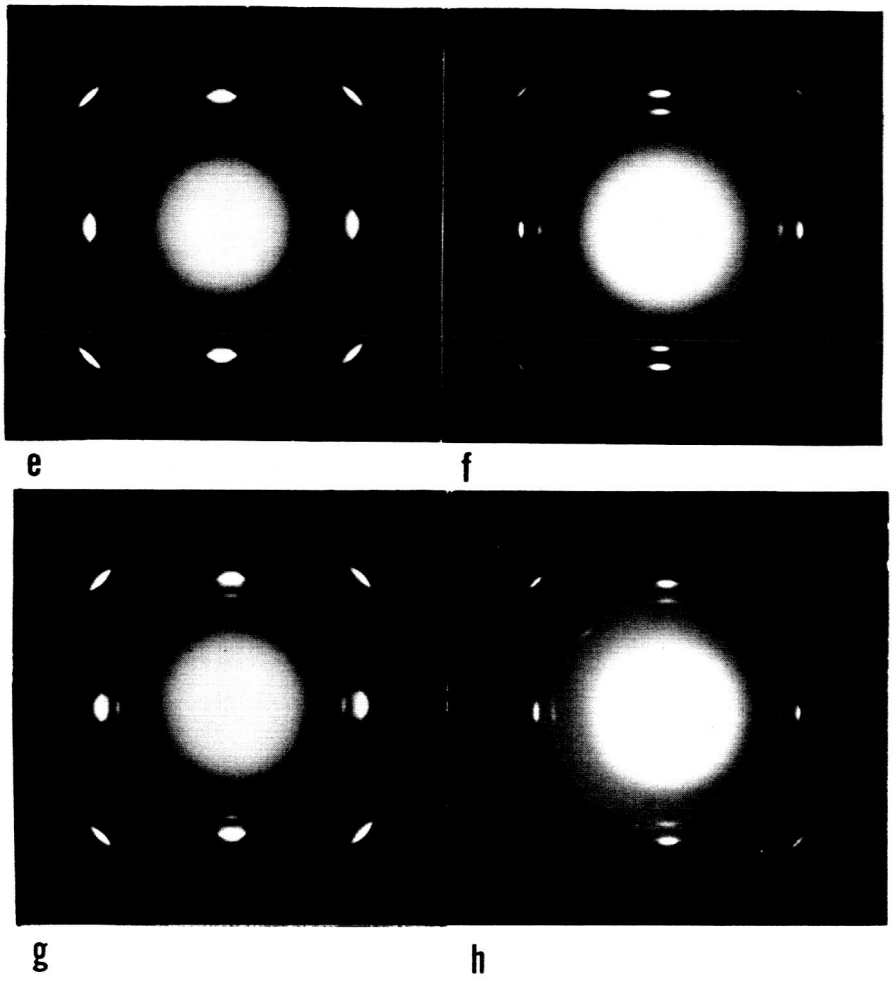

Fig. 4

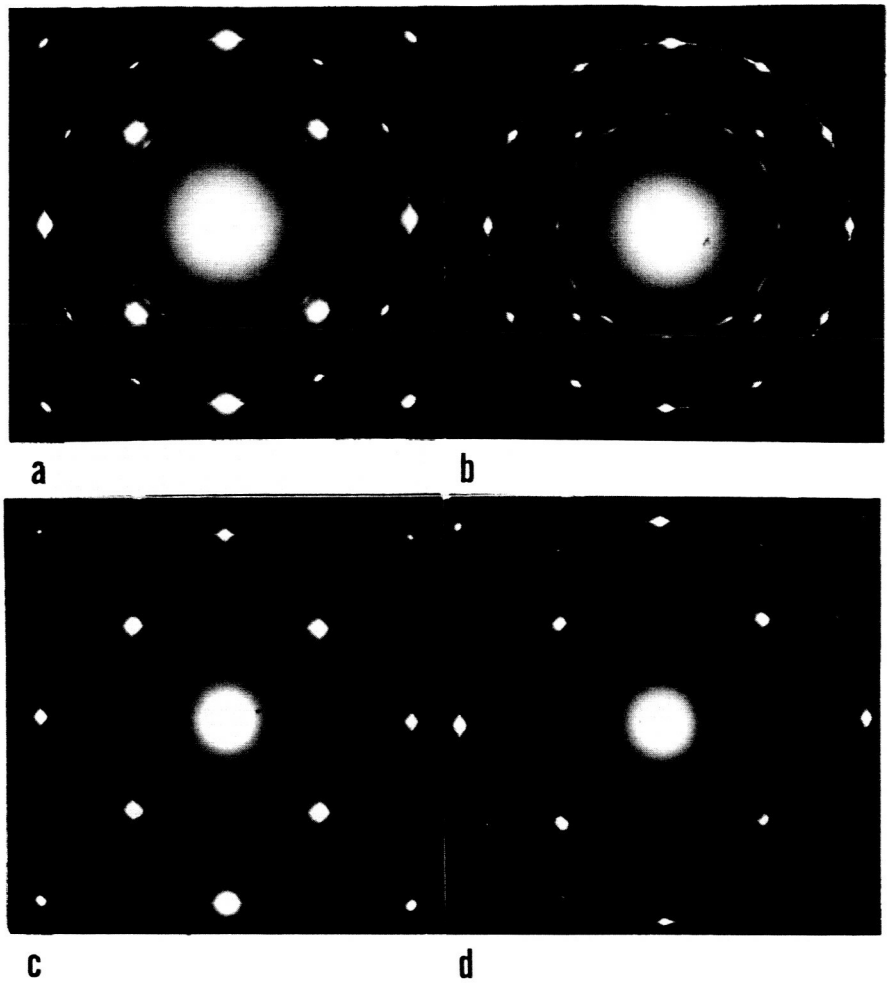

Fig. 5

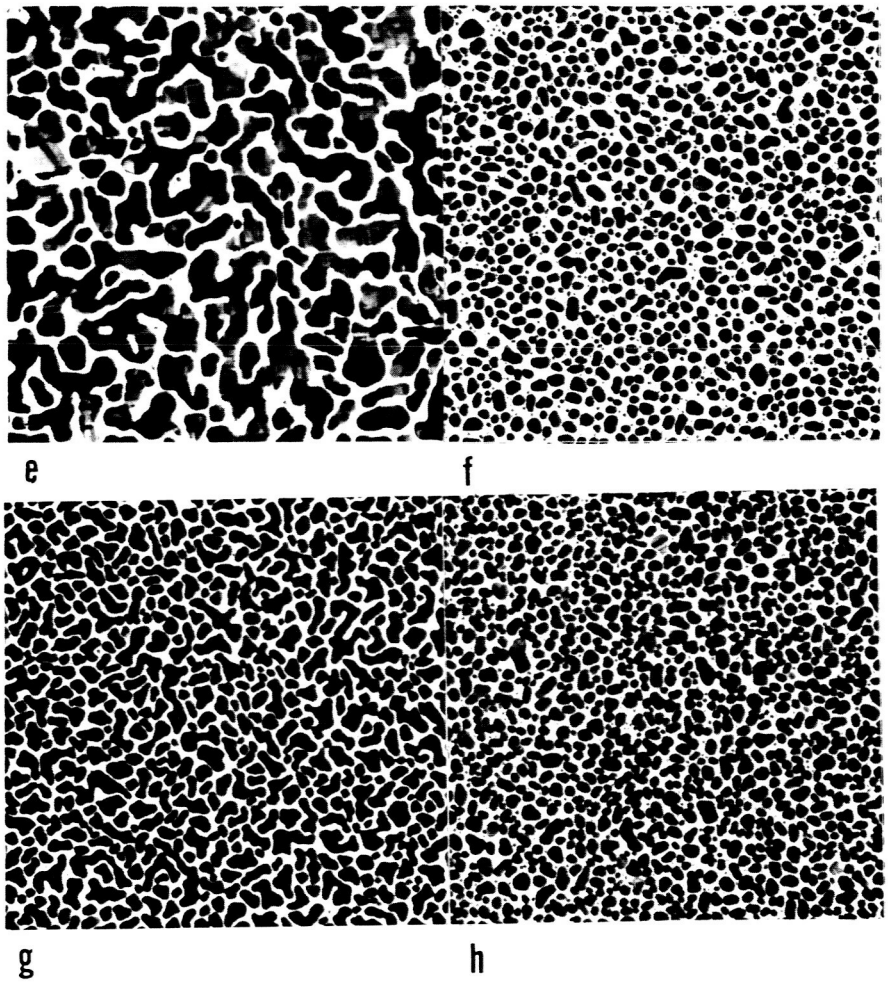

Fig. 5

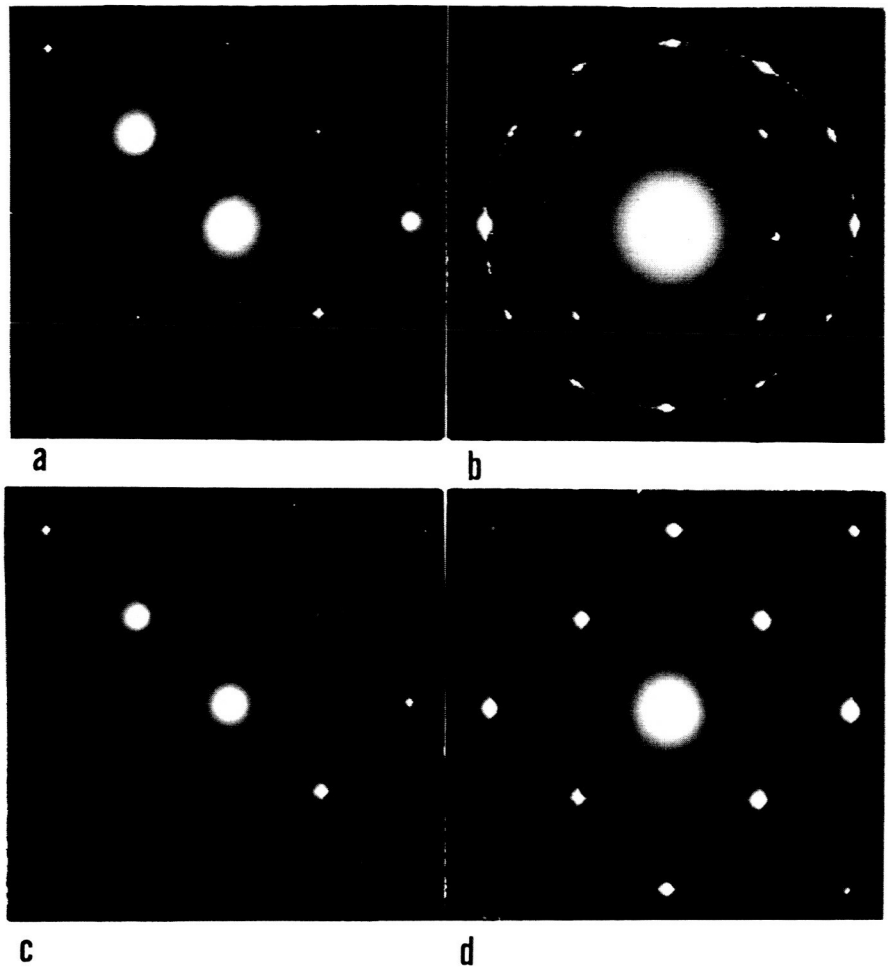

Fig. 6

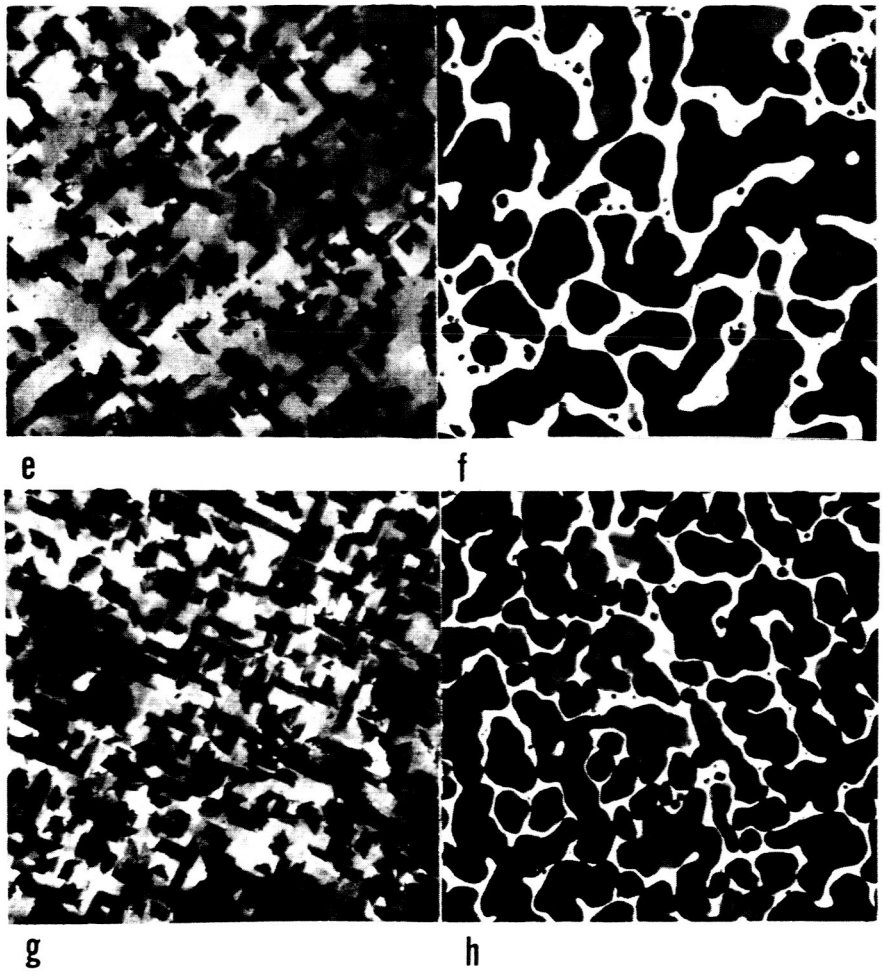

Fig. 6

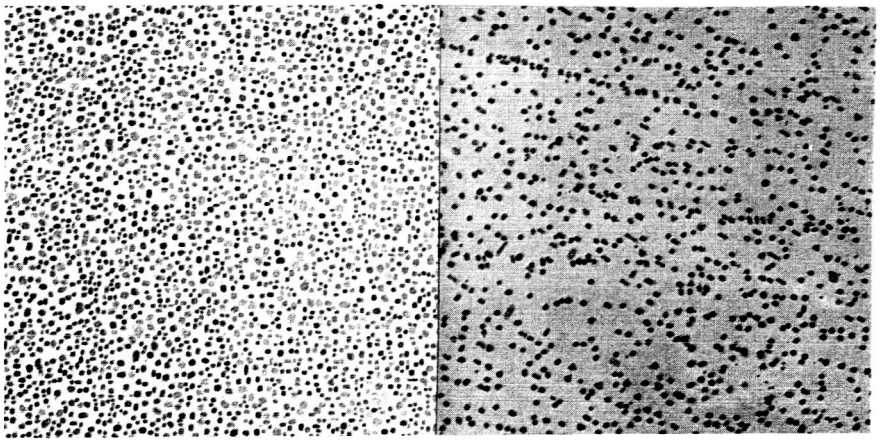

Fig. 7

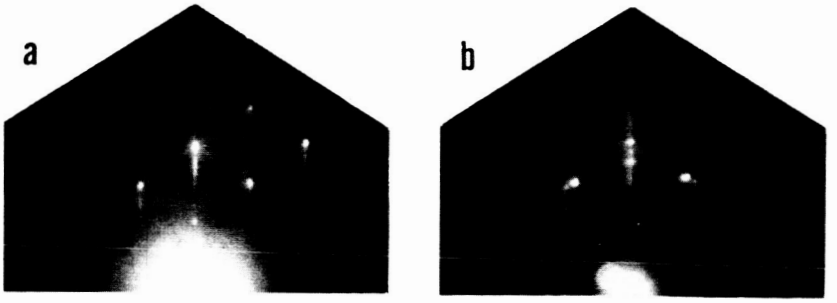

Fig. 8

The Uncertainty Regarding Reconstructed Surfaces*

Comments on L. H. Germer's Letter

In the preceding letter Dr. Germer discusses some experiments with the goal of establishing the reality of reconstruction of metal surfaces upon adsorption of carbon, hydrogen, and oxygen. It is our contention that these experiments can be equally well or better accounted for in terms of unreconstructed surfaces, as suggested earlier[1]).

The observations discussed by Germer can be summarized as follows: at low voltages the additional diffraction spots produced by carbon and hydrogen adsorbed on a nickel {110} surface have the same intensity on the average as the spots already observed in the LEED pattern of the clean surface. Hydrogen cannot be detected on nickel {100} and {111} faces. One-half of a monolayer of oxygen on a tungsten {110} plane produces additional spots with half the intensity of the spots already observed on the clean surface; for three-quarter of a monolayer the intensity ratio between the two kinds of spots is on the average 1:5.

In deducing the reconstructed surface structure ("mixed layer"[1]) from these observations, Germer makes the following assumptions: (1) The diffraction pattern is produced only by the top layer of atoms (except in the case of the three-quarter monolayer of oxygen on tungsten where the second layer contributes to the pattern). (2) Adsorbed carbon, hydrogen, and oxygen have negligible scattering cross sections as compared to nickel and tungsten respectively.

---

* Work supported in part by the National Aeronautics and Space Administration.

Encl. (2)

There is a considerable amount of material available now which indicates that assumption (1) is an unpermissible over-simplification. For instance, three atomic layers have to be taken into account if the intensity versus voltage curve of the (00) beam of a tungsten {110} plane is to be explained by the elementary treatment[2]) used by Germer, which itself is open to criticism. Assumption (2) is inconsistent with assumption (1) because an atom with negligible scattering cross section cannot shield the nickel atom below it from the incident wave. Therefore the nickel atoms in the second layer below the gas atoms should contribute to the diffraction pattern.

In the unreconstructed surface model ("unmixed layer"[1]), the following assumptions are made in interpreting the LEED patterns: (1) The diffraction pattern is produced by several atomic layers not only by primary scattering of the incident wave but to a considerable degree also by secondary scattering which makes it difficult to calculate relative spot intensities even for clean surfaces, not to mention for surfaces covered with adsorption layers. (2) Carbon, hydrogen, and oxygen are partially ionic when adsorbed on many metal surfaces and therefore have a high scattering cross section, especially in the forward direction.

The validity of assumption (1) is well illustrated by the work of Gafner[3]). Assumption (2) appears to be justified for the following reasons: carbon, hydrogen, and oxygen atoms have bound negative ion states with 1.25, .754, and 1.465 eV binding energy respectively. Metal surfaces have regions of surplus negative charge between the surface atoms (see e.g. fig. 3 in ref. (4)). The surplus charge varies with the orientation of the surface and increases from {110} to {100} planes in the b.c.c.

metals and in the sequence {111}, {100}, {110} in the f.c.c. metals. A system consisting of such a metal surface and an atom with a bound negative ion state can achieve a state of lower energy if the atoms are adsorbed in the regions of negative charge surplus and become partially ionic (C^-, H^-, O^-). The variation of surplus charge with surface orientation qualitatively explains why hydrogen can be detected by LEED on nickel {110} planes but not on {100} and {111} planes, and on tungsten {100} planes but not on {110} planes[5]). The difference in binding energy (1.465 versus .754 eV) can explain qualitatively why adsorbed oxygen on the tungsten {110} plane can be detected by LEED, while hydrogen produces no additional spots. The change of the detectability of adsorbed atoms with surface orientation is also qualitatively reasonable from the phenomenological point of view: the probability of electron transfer increases with decreasing work function ({111}→{100}→{110} in f.c.c. metals, {110}→{100} in b.c.c. metals). The decrease of the intensity of the additional spots relative to the intensity of the clean surface spots with increasing number of adsorbed oxygen atoms on the tungsten {110} surface may be attributed to a decrease of the surface charge per oxygen atom which can be caused by mutual depolarization or by the limited negative charge surplus on the surface.

The charge distribution and the resulting scattering potential of such an adsorption layer is difficult to predict. However it seems reasonable to assume that the pseudo-ionic adsorption layer will lead to considerable forward scattering and modulate the incident wave with its periodicity, i.e. the adsorbed atoms do not act as absorbers as assumed by Germer (strong shielding!), but as modulators (negligible shielding!).

As a consequence the unreconstructed nickel or tungsten surface is illuminated by a modulated wave instead of a plane wave which has an effect similar to that of a plane wave illuminating a reconstructed surface. The second effect of the pseudo-ionic adsorption layer is to diffract each diffracted wave leaving the crystal; this can explain the frequently noted relations between the intensity of the different spots[6]. Both phenomena, i.e. modulation of the incident wave by the adsorption layer (primary scattering by adsorbed atoms) and secondary scattering of the diffracted waves by adsorbed atoms (modulation of the diffracted waves by the adsorption layer) occur simultaneously and can lead to a complicated dependence of the relative spot intensities upon voltage.

The arguments given here and elsewhere[1]) should indicate that reconstruction is neither needed to explain the LEED patterns of such surfaces nor is it needed for surface energetic reasons. We contend that the presently available experimental evidence strongly favors unreconstructed surfaces if the choice has to be made between them and reconstructed surfaces. This does not mean that "reconstructed" metal surfaces do not exist. Rather, they are expected to be the rule whenever the bonding between adsorbate atoms is similar in nature and strength to the bonding between adsorbent atoms and between adsorbate and adsorbent atoms. Examples are copper "adsorbed" on a tungsten {110} plane[2]) or silver "adsorbed" on a copper {100} plane[7]). In both cases ordered surface alloys are formed--which requires surface reconstruction--instead of misfitting monolayers (with the normal atomic distances of the adsorbate atoms in the bulk) or of strained monolayers (to fit the atomic arrangement of the crystal surface). Such reconstructed surfaces are quite

obvious from the spot positions (not intensities!) in the LEED patterns and are to be expected on the basis of energetic considerations.

E. BAUER

Michelson Laboratory
China Lake, California 93555

REFERENCES

1) E. Bauer, in Adsorption et Croissance Crystalline, C.N.R.S., Paris (1965) p. 20.

2) N. J. Taylor, Surface Science 4 (1966) 161.

3) G. Gafner, Surface Science 2 (1964) 534.

4) H. J. Juretschke, in The Surface Chemistry of Metals and Semiconductors, ed. by H. C. Gatos (Wiley, New York, 1960) p. 38.

5) P. J. Estrup and J. Anderson, J. Chem. Phys., to be published.

6) E. Bauer, Phys. Rev. 123 (1961) 1206.

7) E. Bauer, unpublished.

An Ultrahigh Vacuum Electron Microscope and Its Application to Work Function Studies

G. Turner and E. Bauer
Michelson Laboratory, China Lake, California 93555

In recent years, the interest in surface phenomena has increased considerably. Of the several methods available for the study of surface phenomena, the interaction of low energy electrons with the surface provides a very powerful tool. With this in mind, an all metal, bakeable, ultrahigh vacuum electron microscope is being developed.[1] The instrument is planned to have several modes of operation, including (1) low energy reflection electron microscopy; (2) low energy electron diffraction; (3) emission microscopy; and (4) mirror microscopy. Presently only the last two modes are being used, together with contact potential and photoelectric work function measurements. Figure 1 shows a view of the instrument. The specimen can be heated to 2800°K by electron bombardment and can be cleaned by ion bombardment. The design of the center electrode of the electrostatic objective lens allows evaporation onto the specimen while in observation position. The base pressure of the system is 2×10^{-10} torr. Residual gases, decomposition and desorption products can be analyzed by means of a mass spectrometer.

The instrument is ideally suited for the study of electron emission phenomena which are well known to be extremely sensitive to residual gases. This is particularly true for the work function minimum observed in many alkali and alkaline earth films and in films of their oxides on refractory metals. The purpose of this study is to determine the relation between

Encl. (3)

properties
the electron emission ^ of surfaces (especially the work function minimum) and the surface structure by combining the techniques discussed above with low energy electron diffraction (LEED). The experimental techniques and the results are illustrated here for the system SrO-W {110} plane.

SrO was evaporated from a Pt ribbon, at a temperature of 1510-1590°K, onto a tungsten single crystal at room temperature. The surface had an orientation near ⟨110⟩ and was cleaned by electron bombardment at 2300°K before deposition. The light from a P.E.K. 110, high pressure, Hg arc lamp was focussed onto the specimen by quartz optics. The photoelectric emission and the photoelectric work function were measured, at intervals during the deposition. The change in contact potential was also measured by the electron beam method. Similar depositions were made in a Varian LEED instrument to obtain information on the atomic arrangement in the surface. Figure 2 illustrates typical results for total photocurrent, photoelectric work function and contact potential change as a function of coverage. No work function minimum is observed. LEED shows that there is no ordered surface structure formed over the whole deposition range. Only an increase in background and a decrease of the intensity of the clean W diffraction spots is noted.

Upon heating such a film, the work function drops from about 2.2 eV at 300°K to approximately 1.7 eV at about 900°K where regions of high emission form at reproducible sites on the W surface (see Fig. 3). In the same temperature range, some new diffraction spots appear above the background of the LEED patterns which are compatible with the patterns expected for several compounds found in the Sr-O-W system including that for epitaxial $SrWO_3$ crystals with perewskite structure with $SrWO_3$ (110) ‖ W(110)

and $SrWO_3$[001] || W[1$\bar{1}$0] and [$\bar{1}$10].[2] This suggests that the high emission centers are $SrWO_3$ crystals. Heating above 950°K leads to an increase in the average work function (~ 2.2 eV at 1000°K) and a decrease in emission current, but the high emission centers persist up to about 1050°K. No major changes in LEED patterns are noticed within this temperature range. At 1050°K the average work function rises sharply to 3.1 eV and the high emission centers disappear and a new structure, as yet unidentified, is observed in the LEED patterns (Fig. 4). This structure persists up to about 1200°K, where it is replaced by one which is also observed in the oxygen-tungsten system, indicating complete removal of Sr. The results depend in detail upon film thickness, specimen history and length of heating period. They can tentatively be interpreted as follows: at 900°K, SrO reacts with W at preferred sites and forms isolated epitaxial $SrWO_3$ crystals with low work function. The rest of the surface stays covered with randomly distributed SrO (work function ~ 2.2 eV) continuously loosing Sr by reduction of SrO at an increasing number of reaction sites. At about 1050°K reaction between SrO and W takes place over the whole surface resulting in the unidentified surface structure having a higher work function. The simultaneous decrease in emission from the $SrWO_3$ crystals may be due to the termination of the Sr supply from the SrO layer.

The work was supported in part by the National Aeronautics and Space Administration.

REFERENCES

1. G. Turner and E. Bauer, J. Appl. Phys. 35, 3080 (1964); (to be published).
2. Deposition at 900°K gives the same LEED pattern as deposition at room temperature with subsequent annealing at 900°K. The LEED pattern obtained after deposition at 1050°K is similar to that of a room temperature deposited film after heating to 1050°K. However it contains a much larger number of spots which allow a more accurate determination of the lateral dimensions of the crystal lattice which turn out not to agree exactly with those of any known structure in the Sr-O-W system.

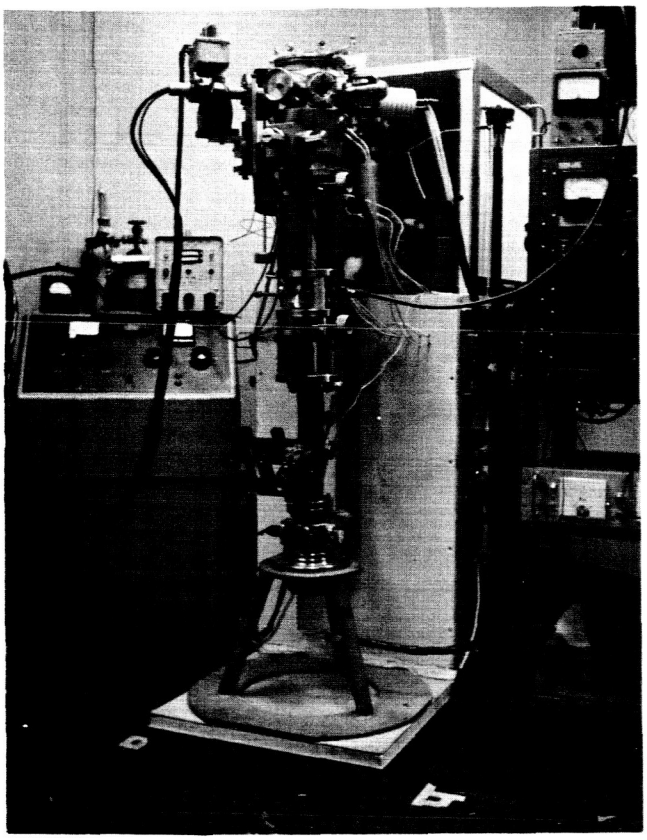

Fig. 1. UHV low energy reflection electron microscope.

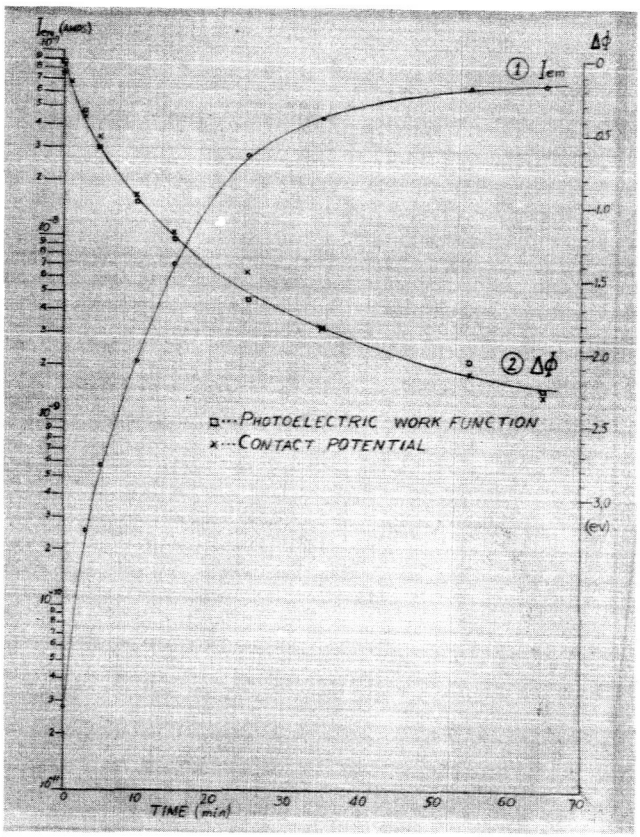

Fig. 2. SrO on W {110}. Curve (1) photoelectroc emission current, Iem, and curve (2) change in photoelectric work function and contact potential as function of deposition time.

Fig. 3. Photoelectric emission micrograph of high emission centers which appear at about 900°K.

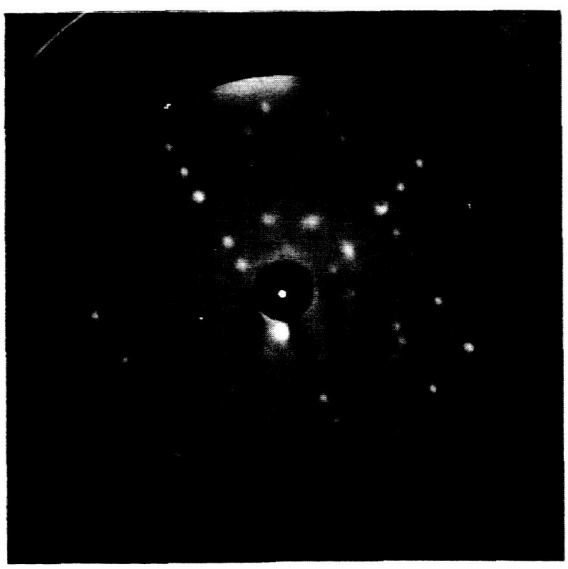

Fig. 4. LEED pattern of unidentified structure appearing at about 1050°K.